Desalination and Water Treatment
www.deswater.com
doi: 10.5004/dwt.2019.23978

152 (2019) 401–410
June

Removal of Remazol Black B from aqueous solution using P-γ-Fe_2O_3 nanoparticles: synthesis, physical characterization, isotherm, kinetic and thermodynamic studies

Shahin Ahmadi[a,*], Abbas Rahdar[b], Somayeh Rahdar[a], Chinenye Adaobi Igwegbe[c,*]

[a]*Department of Environmental Health, Zabol University of Medical Sciences, Zabol, Iran, emails: sh.ahmadi398@gmail.com (S. Ahmadi), rahdar89@gmail.com (S. Rahdar)*
[b]*Department of Physics, University of Zabol, P.O. Box. 35856-98613, Zabol, Iran, email: a.rahdarnanophysics@gmail.com*
[c]*Department of Chemical Engineering, Nnamdi Azikiwe University, Awka, Nigeria, email: ca.igwegbe@unizik.edu.ng*

Received 17 October 2018; Accepted 17 February 2019

ABSTRACT

Dyes found in industrial effluents are one of the most significant hazardous (toxic) materials, therefore its removal before discharge of effluents is essential. The main purpose of this study is to investigate the removal of Remazol Black B (RBB) from its aqueous solution using synthesized P-γ-Fe_2O_3 nanoparticles. The P-γ-Fe_2O_3 nanoparticles were prepared using the surfactant-free electrochemical technique, and characterized for its spectral properties. The influence of different process parameters such as pH (3–12), dosage of P-γ-Fe_2O_3 nanoparticles (0.1–5 g L^{-1}), initial concentration of RBB (50–600 mg L^{-1}), contact time (10–150 min) and solution temperature (298 and 303 K) was studied using the batch adsorption technique. The kinetic, isotherm and thermodynamic parameters were also evaluated. The adsorption efficiency was increased by decreasing the pH of the solution, the dosage of P-γ-Fe_2O_3 nanoparticles, the initial concentration of RBB and the solution temperature. Maximum RBB removal efficiency of 99.74% was attained at the optimum pH of 3, P-γ-Fe_2O_3 nanoparticles dosage of 0.1 g L^{-1}, initial concentration of 100 mg L^{-1}, contact time of 10 min and solution temperature of 298 K. The adsorption of RBB on P-γ-Fe_2O_3 nanoparticles was found to fit best into the pseudo-second-order kinetic model than the pseudo-first-order, which indicates a chemical adsorption process. The adsorption process was best described by the Langmuir adsorption isotherm model with maximum adsorption capacity, q_m of 192.3 mg g^{-1}. The adsorption of RBB on P-γ-Fe_2O_3 was found to be non-spontaneous and endothermic in nature. The results obtained revealed that the synthesized P-γ-Fe_2O_3 nanoparticles could be applied effectively for the removal of RBB from its aqueous solution.

Keywords: Adsorption; Remazol Black B; Aqueous solution; Isotherm; Thermodynamics; Kinetics

1. Introduction

The textile industry makes use of a large number of dyes and produces wastewaters with high concentration of dyes in the range of 10–200 mg L^{-1} [1,2]. The presence of reactive dyes is approximately 4% in these concentrations [3]. Remazol Black B (RBB) is classified as a reactive dye [1,3]. This dye is applied because of its high stability, ease of usage and low energy consumption [3]. It is found in high concentrations in textile wastewaters because of its high solubility in water; however, they cannot be filtered by common system [3,4]. They prevent the full transmission of light into the water bodies and result in the decrease of soluble oxygen and photosynthesis [4]. In addition, eutrophication occurs as a response to the above-mentioned occurrences in water [4,5]. These compounds (dyes) are toxic, allergenic and mutagenic in nature [6,7]. These compounds result in negative effects including the unaesthetic appearance and quality of water

* Corresponding author.

[8]; even a very low dye concentration can make water undesirable for different purposes [9]. Therefore, wastewaters which contain these compounds were highlighted as one of the most hazardous to the environment and public health [3–5,8,10]. Hence, their removal from such wastewaters is important [7].

The methods for dye removal are classified into physical, chemical and biological methods [7,11]. Several methods have been utilized for the management of textile wastewaters including the application of photodecomposition [12], electrolysis [13], adsorption [7,14], oxidation [15], biodegradation [16] and other processes. The adsorption process has been considered as the top method for the removal of color from industrial wastewater [17]. The adsorption process is a physical treatment method in which natural or synthetic adsorbents are used to remove colorful compounds [18]. The adsorption separation method is very effective due to its high efficiency, simplicity, low cost, ease of operation and insensitive to toxic substances [19]. Therefore; several adsorbents for the removal of dyes from effluents have been established. The successful application of the adsorption process is dependent on different parameters such as pH, adsorbent type and the type of pollutant [20].

Different adsorbents have been developed to remove organic and inorganic contaminants [21]. Nanotechnology has provided a new area of research in healthcare [14]. Today, nanotechnology is known as a key and an effective technology in science, technology and industry. It helps to change the atoms and molecules arrangement to achieve a new structure which has not existed before. Nanotechnology has found wide applications in water and wastewater treatment, sewage treatment and purification of air [22,23]. Iron oxide is known as a multitask catalyzer. Iron and its oxides compounds are non-toxic, readily available, cheap and possess good capacity for removing chemical pollutants. Iron oxide has shown good ability in water and wastewater treatments due to their magnetic, oxidative and photocatalytic nature [24–26]. Chen and Li [27] synthesized nanoparticles using $Fe_2(SO_4)_3$ in an alkaline environment and used it for the removal of Cu(II) from an aqueous environment. The size of synthesized nanoparticle was 75 nm and the surface was 24.82 $m^2 g^{-1}$. The efficiency of Cu(II) removal was at an acceptable level. The results showed that the adsorption process followed the pseudo-second-order model. The isothermal studies showed that Langmuir isotherm explained better the adsorption of Cu(II) on α – Fe_2O_3 (with maximum monolayer adsorption capacity of 149.25 mg g^{-1}) than the Freundlich isotherm [27]. Besides, Qu et al. [28] integrated multi-walled carbon nanotubes with Fe_2O_3 nanoparticles and applied it to remove methylene blue and neutral red. The material was found to have a great potential for the removal of organic dyes from polluted water. The researchers demonstrated that equilibrium was attained at 60 min and the adsorption capacities for methylene blue and neutral red were 42.3 and 77.5 mg g^{-1}, respectively [28]. Also, Ranjithkumar et al. [29] studied the removal of acid yellow 17 dye on activated carbon/α-Fe_2O_3 nanocomposite prepared by simple pyrolytic technique via iron (II) gluconate. The adsorption data were found to fit well with the Langmuir, Freundlich and Temkin isotherms at higher dye concentrations. The kinetic data were found to conform to the pseudo-second-order kinetic model. Chen et al. [30] studied the removal of methylene blue (MB) on magnetic γ-Fe_2O_3/SiO_2 (M-γ FS) nanocomposite from aqueous solution. The adsorption of MB was favorable at alkaline condition. The adsorption kinetics data fitted well with the pseudo-second-order kinetic and the Langmuir isotherm models. Adsorption capacity of 25.4, 22.8 and 20.5 mg g^{-1} was obtained at 298, 308 and 318 K, respectively, at initial MB concentration of 180 mg L^{-1}, pH 7, M-γ FS dosage of 2 g L^{-1} and contact time of 4 h.

P-γ-Fe_2O_3 nanocomposite was synthesized (via the surfactant-free electrochemical method), characterized and applied for the removal of Remazol Black B (RBB) dye from its aqueous solution. The impact of various factors such as contact time, adsorbent dosage, initial pH, initial RBB concentration and solution temperature on the removal of RBB using P/γ-Fe_2O_3 nanoparticles was investigated. Their optimum conditions were also determined, which will aid the improvement of the removal of RBB on P/γ-Fe_2O_3 nanoparticles. The isotherm, kinetics and thermodynamics of the adsorption process were also studied.

2. Materials and methods

2.1. Materials

Remazol Black B (RBB) dye (chemical molecular formulae: $C_{26}H_{21}N_5Na_4O_{19}S$) was used as the pollutant. The RBB was purchased from Alvan Sabet Corporation, Hamadan, Iran. All solutions were prepared using de-ionized water. The pH of the solution was adjusted by adding 0.1 N HCl or NaOH solutions. All reagents were of analytical grade and were purchased from Merck (Germany).

2.2. Synthesis of P-γ-Fe_2O_3 nanoparticles

The magnetite nanoparticles were prepared using the surfactant-free electrochemical approach. The synthesis of the nanoparticles was carried out in a closed distilled water system, under ambient atmosphere and temperature. Two steel plates (13 mm × 23 mm × 0.5 mm) were then electroplated with the solution (distilled water) at 10 mA cm^{-2}. The distance between the anode (stainless steel) and the cathode (stainless steel) were varied between 2 and 6 cm for the different preparations. 4 g of iron sulfate ($FeSO_4.7H_2O$) was injected in 200 mL of deionized water (0.072 M) with a low density of 10 mA cm^{-2} in an electrochemical cell [31–33]. After 1.5 h, the anode and replacement cathode were added. A solution of sodium hydroxide, NaOH (1 M) was then added dropwise to bring the pH to the desired level. The electrochemical reaction was then allowed to continue at 10 mA cm^{-2} for 1.5 h before the current was removed. The magnetite nanoparticles (Fe_3O_4 NPs) were isolated with a magnet and washed twice with ethanol and water. 400 mL of distilled water, 20 mL of 1 M HCl solution and 2.5 mL of $Na_2HPO_4.2H_2O$ solution (67 × 10^{-5} M) were added to the solution and stirred for 10 min on a stirrer and exposed to temperature of 100°C for 30 h. Afterward, it was washed several times with water, separated with a magnet and dried at 200°C for 1 h. These factors, such as temperature and lengthy time caused the Fe_3O_4 oxidation and led to the formation of the P-γ-Fe_2O_3 nanocomposites.

2.3. Characterization of P/γ-Fe_2O_3 nanometer-sized particles

The magnetic property of the sample was studied using a vibrating sample magnetometry (VSM, a Kavir Precise Magnetic instrument, Iran). Scanning electron microscopy (TESCAN Mira 3-XMU, USA Inc. instrument capable of 700,000 × magnifications) was used to study the morphology of the nanoparticles. The size of the nanoparticles was obtained through the dynamic light scattering (DLS) tool using a Zetasizer Nano ZS (Malvern Instruments, UK). Fourier-transform infrared spectroscopy of the nanoparticles was done on a JASCO 640 plus machine (4,000–400 cm^{-1}) at room temperature using KBr pellets. X-ray diffraction pattern was obtained via a Philips diffractometer model PW1800 (The Netherlands). The X-ray source was Cukα with 1.541 nm wavelength.

2.4. Experimental procedure and analysis

The effects of different parameters such as pH (3, 5, 7, 9 and 12), dosage of P/γ-Fe_2O_3 nanoparticles (0.1, 0.5, 1, 2, 3 and 5 g L^{-1}), contact time (10, 20, 30, 45, 60, 100, 120 and 150 min), and initial concentration (50, 100, 200, 300 and 500 mg L^{-1}) were investigated on the adsorptive removal of RBB using P-γ-Fe_2O_3 nanoparticles. An initial stock solution of RBB (concentration: 1,000 mg L^{-1}) was prepared with double-distilled water from which other concentrations used in this study were obtained using the dilution method. The batch adsorption experiments were carried out using 250 mL Erlenmeyer flasks. For each adsorption experiment, 100 mL of RBB solution with a known concentration was added into the Erlenmeyer flask. Then, the pH of the solution was adjusted and the adsorbent of known dosage was added to the flask and then mixed with the magnetic stirrer (MODEL: MSH basic) at 150 rpm. The initial and final RBB concentrations were analyzed using a UV–visible recording spectrophotometer (Shimadzu Model: CE-1021-UK), at a wavelength of maximum absorbance, λ_{max} = 578 nm. The removal efficiency, R(%), and the amount of RBB adsorbed, q_e (mg g^{-1}), were calculated based on the following formula [34,35]:

$$\%R = \frac{C_0 - C_f}{C_0} \times 100 \quad (1)$$

where C_0 is the initial RBB concentration and C_f is the final RBB concentration.

$$q_e = \frac{C_0 - C_e}{M} \times V \quad (2)$$

where M is the mass of adsorbent (g), V is the volume of the solution (L), C_0 and C_e are the initial and final or equilibrium liquid phase concentrations of RBB (mg g^{-1}), respectively.

3. Results and discussion

3.1. Physical characterization of the P-γ-Fe_2O_3

The surface morphology of P-γ-Fe_2O_3 nanoparticles (shown in Fig. 1) was obtained via the FE-SEM technique. From Fig. 1, It can be seen that the nanometer-sized composite has a mean diameter of about 50 nm and nearly spherical in shape. Besides, rod-like/needle-like particles can also be observed. The SEM image also shows that the P/γ-Fe_2O_3 nanoparticles are very porous in nature, which will lead to a higher level of contact with the dye [36].

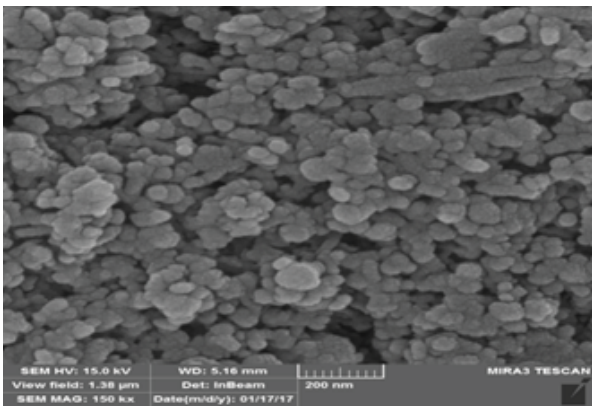

Fig. 1. SEM image of the P-γ-Fe_2O_3 nanoparticles.

The magnetic property of the nanoparticles was confirmed via the VSM tool. Fig. 2 shows the VSM curve of the P-γ-Fe_2O_3 nanoparticles calcined at 200°C measured at room temperature using the VSM tool under the applied magnetic field of 8,000 Oe. As seen in Fig. 2, the VSM curve of the nanoparticles indicates that the P-γ-Fe_2O_3 nanometer-sized particles behave similar to a superparamagnetic material. The magnetic property of a sample makes it easily removed from the water, which reveals its potential as a magnetic adsorbent [37]. Large magnetizations are obtained even for small magnetic fields for ferromagnetic samples [38].

The spectral properties of the adsorbent were determined using the FTIR, which was taken in the range of 400–4,000 cm^{-1} (Fig. 3). Fig. 3 shows the FTIR spectra of the nanoparticles before and after color adsorption. The presence of alkyl halides (C–Br stretching), 1° amine (N–H) bending and alkynes (–C≡C– stretching) was revealed at the band

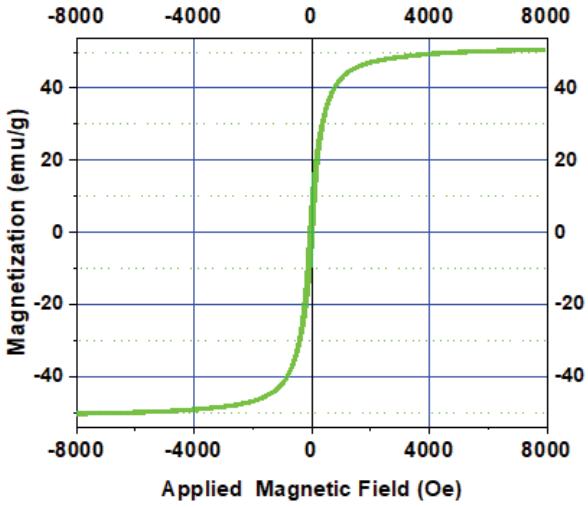

Fig. 2. VSM of the P-γ-Fe_2O_3 nanoparticles.

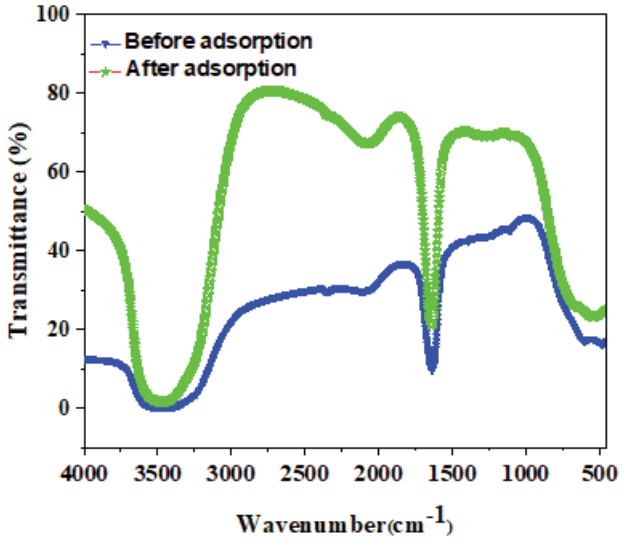

Fig. 3. FTIR spectra of the P-γ-Fe_2O_3 nanoparticles before adsorption and after adsorption.

regions of 481.62, 1,637.76 and 2,021.64 cm^{-1}, respectively. All the aforementioned bands are medium bands. The peak of 3,449.22 cm^{-1} is ascribed to O–H stretch, H–bond of alcohols and phenols, which is a very broad and strong band. This strong band (O–H stretch) contributed actively in the adsorption of RBB. This hydrogen bonding plays a significant role in adsorption processes [39,40]. It is clear from Fig. 3 that the peak intensities shifted after color adsorption on the nanocomposite surface which confirmed the adsorption of RBB on P-γ-Fe_2O_3 nanoparticles. The intensities of the bands increased from 481.62, 1,637.76 and 2,021.64 cm^{-1} to 541.94, 1,639.74 and 2,075.1 cm^{-1}, respectively. The intensity of the O–H band was also increased slightly from 3,449.22 to 3,451.35 cm^{-1}.

The size of the P-γ-Fe_2O_3 nanoparticles before and after adsorption was examined using the DLS (nano-zetasizer) at RT. Figs. 4 and 5 show the size distribution of P-γ-Fe_2O_3 (adsorbent dosage 0.1 g L^{-1}) before and after adsorption at RT, respectively. The results presented in Figs. 4 and 5 conclusively indicate that the size of the nanoparticles increased after adsorption. This may be due to agglomeration of the adsorbent particles after adsorption. Herein, it can be seen that the DLS tool is useful to characterize and obtain the hydrodynamic size of nanoparticles based on their Brownian motion within a nanometer-scale colloidal solution [31,32,41].

To study the crystallographic nature of the P-γ-Fe_2O_3 nanocomposite, the XRD analysis was performed as shown in Fig. 6. From the figure, the diffraction peaks assigned at 2q values of 30.485° (220), 35.744° (311), 43.694° (400), 49.498° (421), 54.233° (422), 57.559° (511) and 62.728° (440) correspond

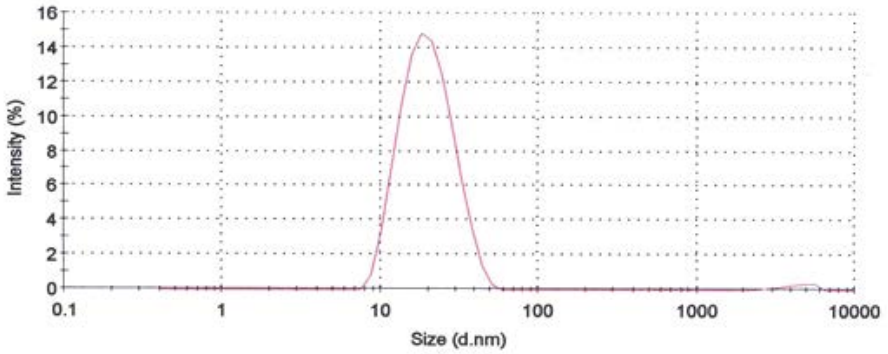

Fig. 4. Size distribution of the nano adsorbent (adsorbent dosage 0.1 g L^{-1}) before adsorption at RT.

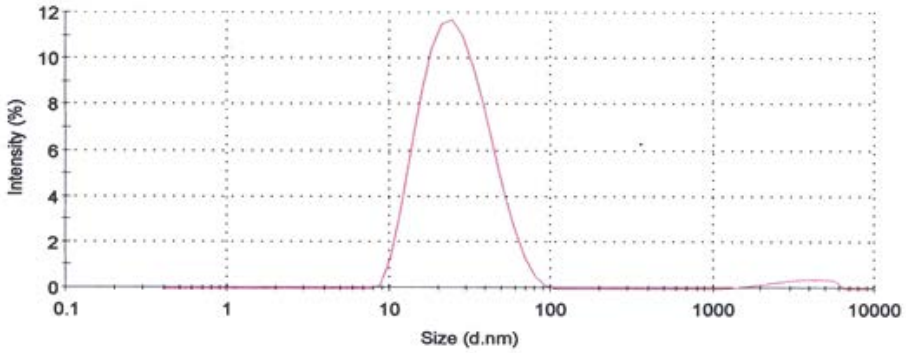

Fig. 5. Size distribution of the nano adsorbent after adsorption at RT.

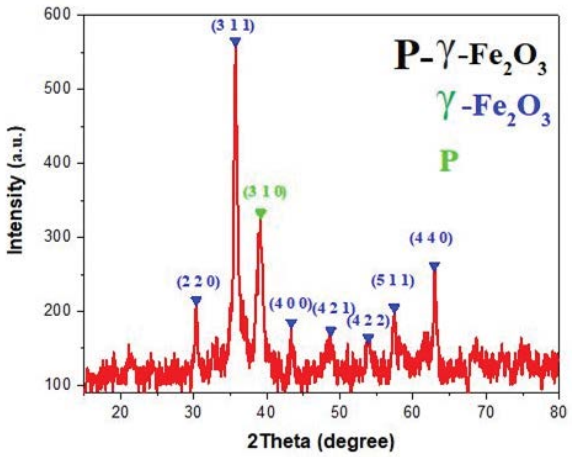

Fig. 6. XRD pattern of P-γ-Fe_2O_3 nanoparticles.

to the Fe_2O_3. The diffraction peaks assigned to the 2q value of 38.784° (310) reflection of *P* can be seen clearly in the P-γ-Fe_2O_3 nanocomposite. It was identified as a cubic crystal system, indicating the presence of the *P* and γ-Fe_2O_3 structures, which is close to the literature data in JCPDS card number for *P* and γ-Fe_2O_3, 002–0266 and 002–1047, respectively. It was selected in the peak search minimum significance of 1.0 Pro-X Perth. This crystalline structure improves the process of adsorption by means of physisorption [33].

3.2. Effect of pH

The effect of pH (3, 5, 7, 9 and 12) on the RBB removal efficiency and adsorption capacity (q_e) is presented in Fig. 7. The adsorption efficiency decreased from 98.2% to 96.66% as the pH increased from 3 to 12. The rate of RBB removal was maximum at pH of 3. Studies have shown that the rate of pollutants removal from an aqueous environment is mainly dependent on the pH of the solution [42]. It could be said that pH is an important factor in dye absorption process [43]. pH has a great influence on the adsorbent superficial load as well as the breakdown of the functional groups on the adsorbent, the chemistry of solution and the level of binding of the adsorbent sites. Changes in pH would influence the process of adsorption and the breakdown of the functional groups on the active adsorbent [42]. The RBB is an anionic dye and the point of zero charge, pH_{ZPC} for P-γ-Fe_2O_3 nanoparticles was found to be 3.8. At pH higher than this value ($pH > pH_{ZPC}$), the surface of the adsorbent (P-γ-Fe_2O_3 nanoparticles) is negatively charged, which led to the attraction of the cations to its surface. At a lower pH ($pH < pH_{ZPC}$), the adsorbent possessed a positive charge [43] and the RBB in aqueous solution is negatively charged. The increase in the adsorption efficiency at lower pH was due to the increase in the number of positively charged sites. Thus, below 3.8, the surface of the P-γ-Fe_2O_3 nanoparticles is positively charged and attracted anions from the dye solution. The adsorption process in different types of anions and cations is different because of the competition for adsorption among the H^+ and OH^- ions with the adsorbate [44]. The adsorption surface showed better performance in adsorption of the anions in low pH in the presence of H^+ ion. However, with the increase in pH and the presence of OH^- ions, the adsorption of cations would be better [42–44].

3.3. Effect of dosage

The effect of adsorbent dose on the removal of RBB and adsorption capacity (q_e) was studied (Fig. 8). It is clear from Fig. 8 that the amount of dye removed decreased as the dosage of nanoparticles increased. Maximum adsorption efficiency and adsorption capacity of 83.76% and 8.37 mg g^{-1} were obtained, respectively, at an adsorbent dose of 0.1 g L^{-1}, which implies that the adsorbent dose of 0.1 g L^{-1} was determined as the optimum dosage. Increasing the adsorbent dose also decreased the efficiency of adsorption; at lower adsorbent dosage, the amount of dye molecules is relatively higher compared with the vacant sites available for adsorption [45].

3.4. Effect of the initial RBB concentration

Fig. 9 shows the effect of initial RBB concentration (50, 100, 200, 300 and 500 mg L^{-1}) on the removal efficiency and adsorption capacity. The adsorption efficiency decreased

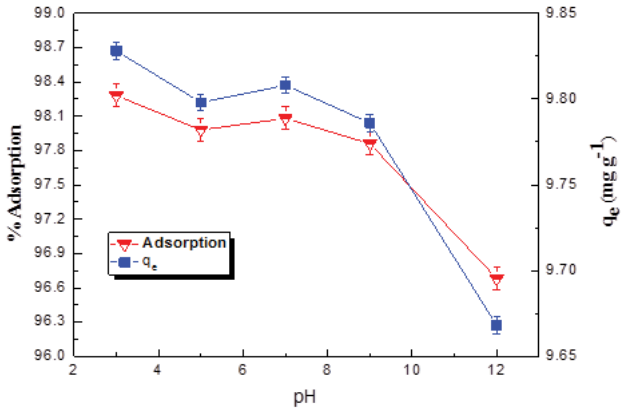

Fig. 7. Effect of pH on adsorption capacity (initial RBB concentration: 100 mg L^{-1}, temperature: 298 K, adsorbent dosage: 0.1 g L^{-1} and time: 10 min).

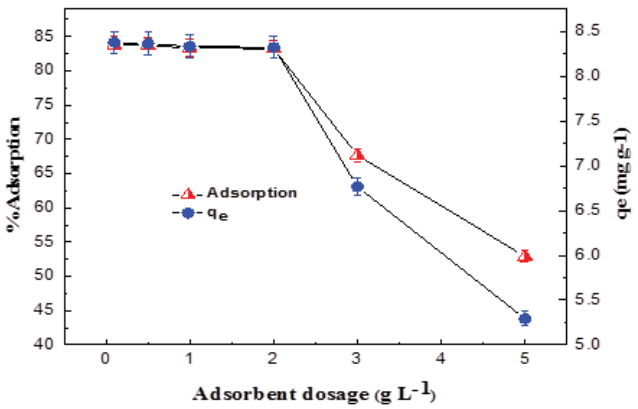

Fig. 8. Effect of adsorbent dose on adsorption capacity (RBB concentration: 100 mg L^{-1}, temperature: 298 K, pH: 3 and time: 10 min).

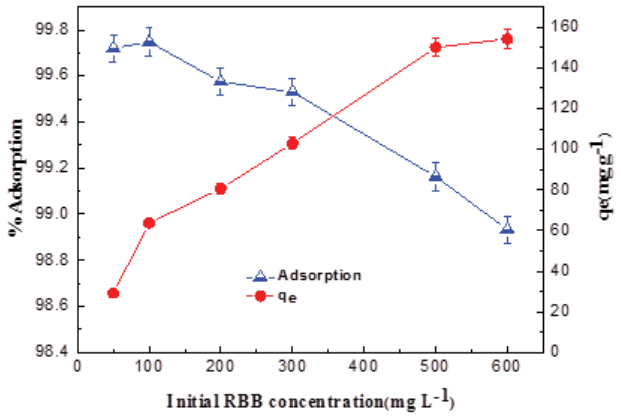

Fig. 9. Effect of initial RBB concentration on adsorption capacity (adsorbent dosage: 0.1 g L^{-1}, temperature: 298 K, pH: 3 and time: 10 min).

from 99.74% to 98.9% with increasing the initial dye concentration from 100 to 600 mg L^{-1}. This is because, during the adsorption process, the surface of the adsorbent was easily saturated by the adsorbate molecules with higher dye concentration. Initially, more adsorption sites were available and after a while, the number of sites for adsorption decreased which led to repulsion between the adsorbed dye molecules on the adsorbent and the dye molecules which are still in solution [46].

3.5. Effect of the time and temperature

Fig. 10 shows the effect of time on the removal of RBB. The figure indicates that the removal efficiency decreased with increasing contact time. Also, the adsorption efficiency increased as temperature decreased. Maximum efficiency

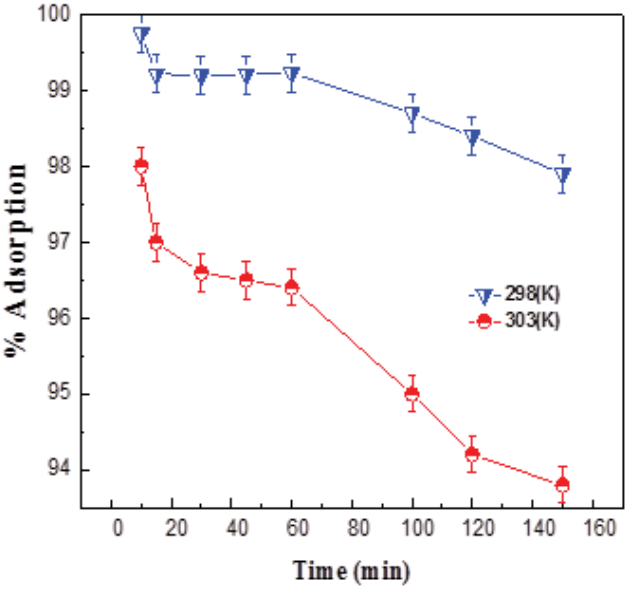

Fig. 10. Effect of time on adsorption capacity (RBB concentration: 100 mg L^{-1}, adsorbent dosage: 0.1 g L^{-1} and pH: 3).

was observed at the contact time of 10 min and temperature of 298 K. Initially, the adsorption process was rapid and became slow until the saturation phase was reached, which lasted for 15 min [47]. Increasing the temperature from 298 to 303 K decreased the removal efficiency. This may be attributed to the fact that a rise in temperature increases the tendency of the dye molecules to escape from the interface, thereby diminishing the rate of sorption. Reduction in adsorption efficiency with increasing temperature indicates the exothermic nature of the adsorption process [28,48].

3.6. Adsorption kinetic studies

Adsorption kinetic models are used to examine the rate of adsorption process and the potential rate controlling step. The two most commonly used kinetic models are the pseudo-first-order and pseudo-second-order kinetic models [49], which were used in this study.

The pseudo-first-order rate equation is expressed as Eq. (3) [47,48]:

$$\log\left(q_e - q_t\right) = \log\left(q_e\right) - \frac{k_1}{2.303} \times t \tag{3}$$

The pseudo-second-order rate equation is given as [48,50]:

$$\frac{t}{q_t} = \frac{1}{\left(k_2 q_e^2\right)} + \frac{t}{q_e} \tag{4}$$

where q_e (mg g^{-1}) and q_t (mg g^{-1}) are the amounts of RBB adsorbed at equilibrium and at time t, respectively; k_1 (min^{-1}) is the pseudo-first-order rate constant of adsorption, and k_2 (g mg^{-1} min^{-1}) is the pseudo-second-order rate constant. The rate constants, k_1 and k_2 were calculated from the plots of log ($q_e - q_t$) vs. t (Fig. 11) and t/q_t vs. t (Fig. 12), respectively.

The pseudo-first-order and pseudo-second-order kinetic plots are presented in Figs. 11 and 12, respectively. The estimated adsorption kinetic parameters are presented in Table 1. The adsorption kinetic data were found to conform best to the pseudo-second-order kinetic model (R^2 = 0.999) compared with the pseudo-first-order model (R^2 = 0.9079), which indicates a chemisorption process [47,51,52].

3.7. Adsorption isotherm studies

Adsorption isotherm is used to describe the relationship between the adsorbate concentration and the amount of adsorbate adsorbed on an adsorbent, q_e [49]. It is assumed to be a key factor in the design of adsorption systems [49]. The two well-known adsorption isotherm models are the Freundlich and Langmuir isotherms. The Langmuir isotherm assumes that the process of adsorption takes places on a monolayer surface while the Freundlich assumes that the adsorption process occurs on a heterogeneous surface [53]. These isotherms were used to determine the relationship between the amount of dye adsorbed and its equilibrium concentration in the solution. For the study, 0.1 g L^{-1}

P-γ-Fe_2O_3 nanoparticles were added to RBB solutions with different concentrations (50–600 mg L^{-1}); the pH of solutions was adjusted to pH 3 and stirred for 10 min.

The Langmuir isotherm model is presented in Eq. (5) [47,48]:

$$\frac{C_e}{q_e} = \frac{1}{q_m} K_L + \frac{C_e}{q_m} \quad (5)$$

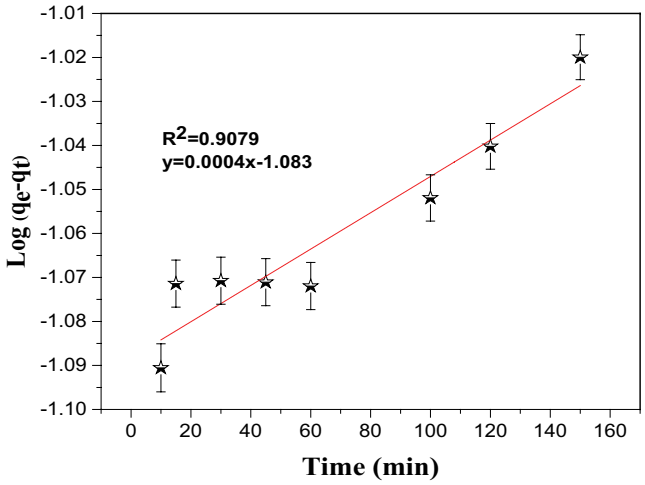

Fig. 11. Pseudo-first-order model plot of RBB adsorption on P-γ-Fe_2O_3 nanoparticles. (adsorbent dosage 0.1 g L^{-1})

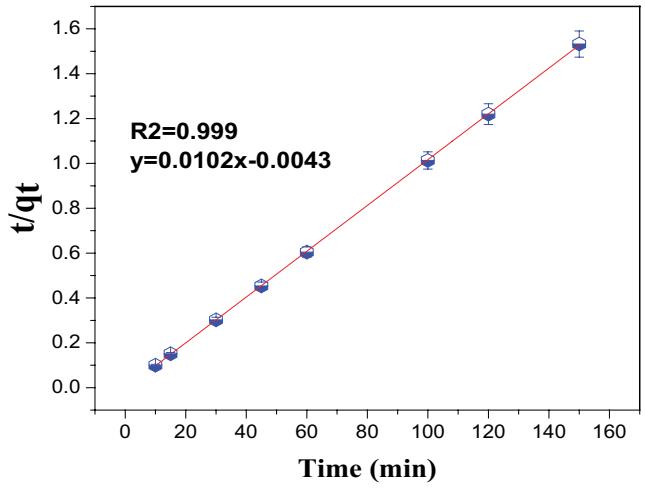

Fig. 12. Pseudo-second-order model plot of RBB adsorption on P-γ-Fe_2O_3 nanoparticles.

Table 1
Calculated kinetic parameters for the adsorption of RBB onto P-γ-Fe_2O_3 nanoparticles

Pseudo-first-order		Pseudo-second-order	
q_e	0.081	q_e	98.04
k_1	0.0009	k_2	0.024
R_2	0.9079	R^2	0.999

where q_e is the RBB uptake by the P-γ-Fe_2O_3 nanoparticles, q_m is the maximum adsorption capacity (mg g^{-1}), K_L (L mg^{-1}) is the Langmuir isotherm constant related to the affinity of the binding sites and energy of adsorption. K_L is also a constant that rises when the dosage of adsorbent is increased [54].

The Freundlich isotherm is stated as Eq. (6) [46,52]:

$$\log q_e = \frac{1}{n} \log C_e + \log k_f \quad (6)$$

where q_e is the amount of RBB adsorbed, C_e is the equilibrium concentration of RBB in the solution; and k_f (mg g^{-1}) (L mg^{-1}) and n are constants incorporating the factors affecting the adsorption capacity and intensity of adsorption, respectively.

The estimated isotherm parameters and their respective correlation coefficients, R^2, are presented in Table 2. The isotherm data were found to conform more to the Langmuir isotherm compared with the Freundlich isotherm with regards to their correlation coefficients, R^2, (Table 2). According to the results obtained (Table 2; Figs. 13 and 14), this study is more compatible with the Langmuir isotherm (R^2 = 0.9517) with monolayer adsorption capacity, q_m of 192.3 mg g^{-1}. The adsorption intensity, n was obtained as 2.058, which lies within 1–10 range ($1 < n < 10$) suggesting that the adsorption of RBB onto P-γ-Fe_2O_3 is favorable [55]. The dimensionless parameter, R_L, was also calculated. The R_L value of 0.552 indicates that the adsorption process is favorable since the value lies between 0 and 1 ($0 < R_L < 1$) [9].

Table 2
Isotherms parameters for adsorption of RBB onto P/γ-Fe_2O_3 nanoparticles

Langmuir		Freundlich	
q_m (mg g^{-1})	192.3	k_f (mg g^{-1})	8.277
K_L (L mg^{-1})	0.0081	n	2.058
R^2	0.9517	R^2	0.9275
R_L	0.552	–	–

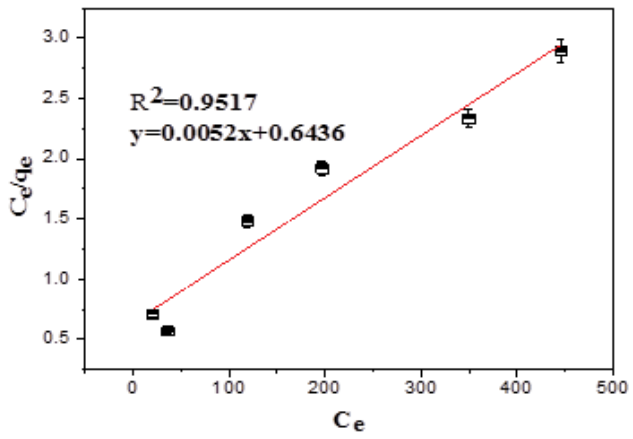

Fig. 13. Langmuir model plot of RBB adsorption on P-γ-Fe_2O_3 nanoparticles.

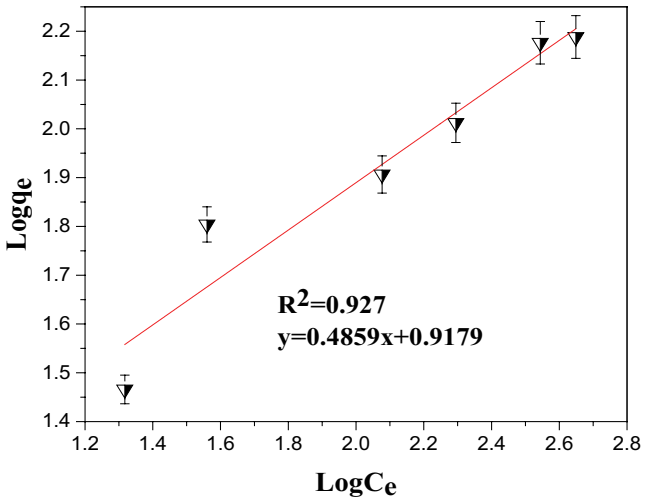

Fig. 14. Freundlich model plot of RBB adsorption on P-γ-Fe_2O_3 nanoparticles.

3.8. Thermodynamic study

The three basic parameters for thermodynamic study are standard enthalpy (Δ*H*°), Gibbs free energy (Δ*G*°) and standard entropy (Δ*S*°). The free energy change can be determined using Eq. (7) [28]:

$$\Delta G^\circ = -RT\ln K \tag{7}$$

where Δ*G*° is the free energy change of sorption process (kJ mol^{-1}), *K* is the equilibrium constant, *T* is the temperature in K and *R* is the universal gas constant (8.314 J mol^{-1} K^{-1}).

The free energy change can be also expressed in terms of enthalpy change of sorption as a function of temperature and is stated as follows [56–59]:

$$\Delta G^\circ = \Delta H^\circ - T\Delta S^\circ \tag{8}$$

The values of Δ*H*° and Δ*S*° can be calculated using Eq. (9) [60,61]:

$$\ln K_L = \frac{\Delta S^\circ}{R} - \frac{\Delta H^\circ}{RT} \tag{9}$$

The Δ*H*° and Δ*S*° values (Table 3) was determined from the slope and intercept of the linear plot of Ln *K* vs. 1/*T* (Van't Hoff plot), respectively. The value of Δ*H*° was found to be 3.532 kJ mol^{-1}. Δ*G*° values were obtained as 12.38 and 12.59 kJ mol^{-1} at temperatures of 298 and 303 K, respectively (Table 3). The positive value of Δ*H*° indicates that the process of RBB adsorption is endothermic in nature [49,50]. The positive value of Δ*G*° at all temperatures denotes random feasibility [62] and the adsorption was not favorable at a higher temperature. Also, the negative value of Δ*S*° was caused by the decrease in efficiency of the reaction to higher temperature [63]. The negative Δ*S*° showed that the ordered arrangement at the solid–liquid interface increases during the process of adsorption [30].

Table 3
Thermodynamic parameters for RBB adsorption on P-γ-Fe_2O_3 nanoparticles

Temperature (K)	Δ*G*° (kJ mol^{-1})	Δ*H*° (kJ mol^{-1})	Δ*S*° (kJ mol K^{-1})
298	12.38	3.532	–0.029
303	12.59		

4. Conclusion

The effectiveness of P-γ-Fe_2O_3 nanoparticles on the adsorptive removal of Remazol Black B (RBB) from its aqueous solution was investigated. The impact of pH, dosage of P-γ-Fe_2O_3 nanoparticles, contact time, initial concentration and temperature on the removal of RBB was studied using the batch adsorption technique. The thermodynamics, kinetics and isotherm of the RBB adsorption process were studied. The process of adsorption was improved by decreasing the pH of the solution, P-γ-Fe_2O_3 nanoparticles dosage, initial concentration of RBB and solution temperature. Maximum removal of 99.47% was reached at an adsorbent dosage of 0.1 g L^{-1}, temperature of 298 K, pH of 3, and time of 10 min. The experimental data were found to be more compatible with the Langmuir isotherm (with maximum adsorption capacity, q_m of 192.3 mg g^{-1}) and pseudo-second-order kinetc models. The RBB adsorption was found to be endothermic and non-spontaneous in nature. The results obtained showed that the P-γ-Fe_2O_3 nanoparticles could be effectively utilized for the removal of RBB from an aqueous environment.

Acknowledgments

The authors are grateful to the Zabol University of Medical Sciences for their financial support (Grant no. 1396.274).

References

[1] A. Fernandes, A. Morao, M. Magrinho, A. Lopes, I. Gonçalves, Electrochemical degradation of C.I. acid orange 7, Dyes Pigm., 61 (2004) 287–296.
[2] S. Ahmadi, L. Mohammadi, C.A. Igwegbe, S. Rahdar, A.M. Banach, Application of response surface methodology in the degradation of Reactive Blue 19 using H_2O_2/MgO nanoparticles advanced oxidation process, Int. J. Ind. Chem., 10 (2018) 1–3.
[3] S. Ahmadi, F.K. Mostafapour, Treatment of textile wastewater using a combined coagulation and DAF processes, Iran, 2016, Arch. Hyg. Sci., 6 (2017) 229–234.
[4] D. Pokhrel, T. Viraraghavan, Treatment of pulp and paper mill wastewater—a review, Sci. Total Environ., 333 (2004) 37–58.
[5] V. López-Grimau, M.C. Gutierrez, Decolourisation of simulated reactive dyebath effluents by electrochemical oxidation assisted by UV light, Chemosphere, 62 (2006) 106–112.
[6] M. Kamranifar, A. Naghizadeh, Montmorillonite nanoparticles in removal of textile dyes from aqueous solutions: study of kinetics and thermodynamics, Iran. J. Chem. Chem. Eng., 36 (2017) 127–137.
[7] A. Naghizadeh, R. Nabizadeh, Removal of reactive blue 29 dye by adsorption on modified chitosan in the presence of hydrogen peroxide, Environ. Prot. Eng., 42 (2016) 149–168.
[8] A.H. Abdullah, W.Y. Wong, M.I. Yaziz, Decolorization of reactive orange 16 dye by copper oxide system, Sains Malaysiana, 39 (2010) 587–591.

[9] C.A. Igwegbe, P.C. Onyechi, O.D. Onukwuli, I.C. Nwokedi, Adsorptive treatment of textile wastewater using activated carbon produced from *Mucuna pruriens* seed shells, World J. Eng. Technol., 4 (2016) 21–37.
[10] I. Arslan-Alaton, I. Kabdaşlı, B. Vardar, O. Tünay, Electrocoagulation of simulated reactive dyebath effluent with aluminum and stainless steel electrodes, J. Hazard. Mater., 164 (2009) 1586–1594.
[11] T. Robinson, G. McMullan, R. Marchant, P. Nigam, Remediation of dyes in textile effluent: a critical review on current treatment technologies with a proposed alternative, Bioresour. Technol., 77 (2001) 247–255.
[12] E. Bazrafshan, A.A. Zarei, H. Nadi, M.A. Zazouli, Adsorptive removal of methyl orange and reactive red 198 dyes by *Moringa peregrina* ash, Indian J. Chem. Technol., 2 (2014) 105–113.
[13] T.A. Albanis, D.G. Hela, T.M. Sakellarides, T.G. Danis, Removal of dyes from aqueous solutions by adsorption on mixtures of fly ash and soil in batch and column techniques, Global Nest J., 2 (2000) 237–244.
[14] B. Royer, N.F. Cardoso, E.C. Lima, T.R. Macedo, C. Airoldi, A useful organofunctionalized layered silicate for textile dye removal, J. Hazard. Mater., 181 (2010) 366–374.
[15] S. Ahmadi, F. KordMostafapour, Adsorptive removal of aniline from aqueous solutions by *Pistacia atlantica* (Baneh) shells: isotherm and kinetic studies, J. Sci. Technol. Environ. Inf., 5 (2017) 327–335.
[16] K.V. Kumar, V. Ramamurthi, S. Sivanesan, Biosorption of malachite green, a cationic dye onto *Pithophora* sp., a fresh water algae, Dyes Pigm., 69 (2006) 102–107.
[17] R.V. Kandisa, K.V. Narayana Saibaba, K.B. Shaik, R. Gopinath, Dye removal by adsorption: a review, J. Biorem. Biodegrad., 7 (2016) 6.
[18] X. Florenza, A.M. Solano, F. Centellas, C.A. Martínez-Huitle, E. Brillas, S. Garcia-Segura, Degradation of the azo dye Acid Red 1 by anodic oxidation and indirect electrochemical processes based on Fenton's reaction chemistry. Relationship between decolorization, mineralization and products, Electrochim. Acta, 142 (2014) 276–288.
[19] D. Pathania, S. Sharma, P. Singh, Removal of methylene blue by adsorption onto activated carbon developed from *Ficus carica* bast, Arabian J. Chem., 10 (2017) S1445–S1451.
[20] E. Derakhshani, A. Naghizadeh, Optimization of humic acid removal by adsorption onto bentonite and montmorillonite nanoparticles, J. Mol. Liq., 259 (2018) 76–81.
[21] S. Rahdar, A. Rahdar, C.A. Igwegbe, F. Moghaddam, S. Ahmadi, Synthesis and physical characterization of nickel oxide nanoparticles and its application study in the removal of ciprofloxacin from contaminated water by adsorption: equilibrium and kinetic studies, Desal. Wat. Treat., 141 (2019) 386–393.
[22] B. Bestani, N. Benderdouche, B. Benstaali, M. Belhakem, A. Addou, Methylene blue and iodine adsorption onto an activated desert plant, Bioresour. Technol., 99 (2008) 8441–8444.
[23] S. Ahmadi, A. Banach, F.K. Mostafapour, D. Balarak, Study survey of cupric oxide nanoparticles in removal efficiency of ciprofloxacin antibiotic from aqueous solution: adsorption isotherm study, Desal. Wat. Treat., 89 (2017) 297–303.
[24] M. Taheri, M.A. Moghaddam, M. Arami, Techno-economical optimization of Reactive Blue 19 removal by combined electrocoagulation/coagulation process through MOPSO using RSM and ANFIS models, J. Environ. Manage., 128 (2013) 798–806.
[25] M. Hepel, J. Luo, Photoelectrochemical mineralization of textile diazo dye pollutants using nanocrystalline WO_3 electrodes, Electrochim. Acta, 47 (2001) 729–740.
[26] H. Inan, A. Dimoglo, H. Şimşek, M. Karpuzcu, Olive oil mill wastewater treatment by means of electro-coagulation, Sep. Purif. Technol., 36 (2004) 23–31.
[27] Y.H. Chen, F.A. Li, Kinetic study on removal of copper(II) using goethite and hematite nano-photocatalysts, J. Colloid Interface Sci., 347 (2010) 277–281.
[28] S. Qu, F. Huang, S. Yu, G. Chen, J. Kong, Magnetic removal of dyes from aqueous solution using multi-walled carbon nanotubes filled with Fe_2O_3 particles, J. Hazard. Mater., 160 (2008) 643–647.
[29] V. Ranjithkumar, S. Sangeetha, S. Vairam, Synthesis of magnetic activated carbon/α-Fe_2O_3 nanocomposite and its application in the removal of acid yellow 17 dye from water, J. Hazard. Mater., 29 (2014) 127–135.
[30] D. Chen, Z. Zeng, Y. Zeng, F. Zhang, M. Wang, Removal of methylene blue and mechanism on magnetic γ-Fe_2O_3/SiO_2 nanocomposite from aqueous solution, Water Resour. Ind., 15 (2016) 1–13.
[31] S.M. Taimoory, J.F. Trant, A. Rahdar, M. Aliahmad, F. Sadeghfar, M. Hashemzaei, Importance of the inter-electrode distance for the electrochemical synthesis of magnetite nanoparticles: synthesis, characterization, computational modelling, and cytotoxicity, e-J. Surf. Sci. Nanotechnol., 15 (2017) 31–39.
[32] S. Rahdar, C.A. Igwegbe, A. Rahdar, S. Ahmadi, Efficiency of sono-nano-catalytic process of magnesium oxide nano particle in removal of penicillin G from aqueous solution, Desal. Wat. Treat., 106 (2018) 330–335.
[33] N.A. Elnasri, M.A. Elsheik, M.A. Eltayeb, Physico-chemical characterization and Freundlich isotherm studies of adsorption of Fe(II), from aqueous solution by using activated carbon prepared from *Doum* fruit waste, Arch. Appl. Sci. Res., 5 (2013) 149–158.
[34] S.M. Taimoory, A. Rahdar, M. Aliahmad, F. Sadeghfar, M.R. Hajinezhad, M. Jahantigh, P. Shahbazi, J.F. Trant, The synthesis and characterization of a magnetite nanoparticle with potent antibacterial activity and low mammalian toxicity, J. Mol. Liq., 265 (2018) 96–104.
[35] S. Ahmadi, F.K. Mostafapoor, Adsorptive removal of Bisphenol A from aqueous solutions by Pistacia atlantica: isotherm and kinetic studies, Pharm. Chem. J., 4 (2017) 1–8.
[36] S. Banerjee, M.C. Chattopadhyaya, Adsorption characteristics for the removal of a toxic dye, tartrazine from aqueous solutions by a low cost agricultural by-product, Arabian J. Chem., 10 (2017) S3381–S3393.
[37] Y. Liu, Y. Li, Xinzhao, W. Chi, Q. Huang, C. Yu, Y. Xiang, Effect of magnetite nanoparticles on dye absorption properties of magnetite carbon composites, Bull. Mater. Sci., 40 (2017) 367–373.
[38] B. Issa, I.M. Obaidat, B.A. Albiss, Y. Haik, Magnetic nanoparticles: surface effects and properties related to biomedicine applications, Int. J. Mol. Sci., 14 (2013) 21266–21305.
[39] X. Zhang, X. Wang, Z. Chen, A novel nanocomposite as an efficient adsorbent for the rapid adsorption of Ni(II) from aqueous solution, Materials, 10 (2017) 1124.
[40] F. Batool, J. Akbar, S. Iqbal, S. Noreen, S.N.A. Bukhari, Study of isothermal, kinetic, and thermodynamic parameters for adsorption of cadmium: an overview of linear and nonlinear approach and error analysis, Bioinorg. Chem. Appl., (2018) Article ID: 3463724, 11 p.
[41] M. Aliahmad, A. Rahdar, F. Sadeghfar, S. Bagheri, M.R. Hajinezhad, Synthesis and biochemical effects of magnetite nanoparticle by surfactant-free electrochemical method in an aqueous system: the current density effect, Nanomed. Res. J., 1 (2016) 39–46.
[42] S. Ahmadi, F.K. Mostafapour, Survey of efficiency of dissolved air flotation in removal penicillin G potassium from aqueous solutions, Br. J. Pharm. Res., 15 (2017) 1–11.
[43] S. Ahmadi, C.A. Igwegbe, Adsorptive removal of phenol and aniline by modified bentonite: adsorption isotherm and kinetics study, Appl. Water Sci., 8 (2018) 170.
[44] A. Dalvand, M. Gholami, A. Joneidi, N.M. Mahmoodi, Investigation of electrochemical coagulation process efficiency for removal of reactive red 198 from colored wastewater, J. Color Sci. Technol., 3 (2009) 97–105.
[45] E. Khosla, S. Kaur, P.N. Dave, Mechanistic study of adsorption of acid orange-7 over aluminum oxide nanoparticles, J. Eng., 2013 (2013) Article ID: 593534, 8 p.
[46] H. Hemmati, E. Bazrafshan, H. Kamani, J. Mosafer, D. Balarak, F.K. Mostafapour, Optimization of sono-nanocatalytic process using γ-Fe_2O_3 for Penicillin antibiotic removal by response surface methodology, J. Torbat Heydariyeh Univ. Med. Sci., 5 (2017) 1–16.

[47] N. Khoshnamvand, S. Ahmadi, F.K. Mostafapour, Kinetic and isotherm studies on Ciprofloxacin an adsorption using magnesium oxide nanoparticles, J. Appl. Pharm. Sci., 7 (2017) 79–83.
[48] S. Wu, X. Zhao, Y. Li, C. Zhao, Q. Du, J. Sun, Y. Wang, X. Peng, Y. Xia, Z. Wang, L. Xia, Adsorption of ciprofloxacin onto biocomposite fibers of graphene oxide/calcium alginate, Chem. Eng. J., 230 (2013) 389–395.
[49] A. Naghizadeh, M. Ghafouri, A. Jafari, Investigation of equilibrium, kinetics and thermodynamics of extracted chitin from shrimp shell in Reactive Blue 29 (RB-29) removal from aqueous solutions, Desal. Wat. Treat., 70 (2017) 355–363.
[50] A. Naghizadeh, F. Ghasemi, E. Derakhshani, H. Shahabi, Thermodynamic, kinetic and isotherm studies of sulfate removal from aqueous solutions by graphene and graphite nanoparticles, Desal. Wat. Treat., 80 (2017) 247–254.
[51] C.A. Igwegbe, O.D. Onukwuli, J.T. Nwabanne, Adsorptive removal of vat yellow 4 on activated *Mucuna pruriens* (Velvet bean) seed shells carbon, Asian J. Chem. Sci., 1 (2016) 1–16.
[52] M. Al-Ghouti, M.A. Khraisheh, N.M. Ahmad, S. Allen, Thermodynamic behaviour and the effect of temperature on the removal of dyes from aqueous solution using modified diatomite: a kinetic study, J. Colloid Interface Sci., 287 (2013) 6–13.
[53] S. Ahmadi, S. Rahdar, C.A. Igwegbe, A. Rahdar, N. Shafighi, F. Sadeghfar, Data on the removal of fluoride from aqueous solutions using synthesized P/γ-Fe_2O_3 nanoparticles: a novel adsorbent, MethodsX, 6 (2019) 98–106.
[54] A. Naghizadeh, Comparison between activated carbon and multiwall carbon nanotubes in the removal of cadmium(II) and chromium(VI) from water solutions, J. Water Supply Res. Technol. AQUA, 64 (2015) 64–73.
[55] M.C. Menkiti, A.O. Okoani, M.I. Ejimofor, Adsorptive study of coagulation treatment of paint wastewater using novel *Brachystegia eurycoma* extract, Appl. Water Sci., 8 (2018) 189.
[56] V.K. Gupta, I. Ali, K. Vipin, Adsorption studies on the removal of Vertigo Blue 49 and Orange DNA13 from aqueous solutions using carbon slurry developed from a waste material, J. Colloid Interface Sci., 315 (2007) 87–96.
[57] J.W. Lee, S.P. Choi, R. Thiruvenkatachari, W.G. Shim, H. Moon, Evaluation of the performance of adsorption and coagulation processes for the maximum removal of reactive dyes, Dyes Pigm., 69 (2006) 196–203.
[58] E. Bazrafshan, F.K. Mostafapour, A.H. Mahvi, Phenol removal from aqueous solutions using pistachio-nut shell ash as a low cost adsorbent, Fresenius Environ. Bull., 21 (2012) 2962–2968.
[59] H. Biglari, Evaluation of phenol removal from aqueous solution by banana leaf ash, J. Global Pharm. Technol., 9 (2017) 20–28.
[60] M. Rafiee, M. Jahangiri-rad, Adsorption of reactive blue 19 from aqueous solution by carbon nano tubes: equilibrium, thermodynamics and kinetic studies, Res. J. Environ. Sci., 8 (2014) 205–214.
[61] C.A. Onyechi, Textile Wastewater Treatment Using Activated Carbon from Agro-Wastes, Master of Engineering Thesis, Department of Chemical Engineering, Nnamdi Azikiwe University, Awka, Nigeria, 2014.
[62] P.K. Sharma, S. Ayub, C.N. Tripathi, Isotherms describing physical adsorption of Cr(VI) from aqueous solution using various agricultural wastes as adsorbents, Cogent Eng., 3 (2016).
[63] M.A. Behnajady, N. Modirshahla, F. Ghanbary, A kinetic model for the decolorization of C.I. Acid Yellow 23 by Fenton process, J. Hazard. Mater., 148 (2007) 98–102.